Article

Dy-Modified Mn/TiO₂ Catalyst Used for the Selective Catalytic Reduction of NO in Ammonia at Low Temperatures

Bing Xu *, Zhen Wang, Jie Hu, Lei Zhang [ID], Zhipeng Zhang, Hongtan Liang, Yong Zhang and Guozhi Fan

Hubei Provincial Engineering Technology Research Center of Agricultural and Sideline Resources, Chemical Engineering and Utilization, School of Chemistry and Environmental Engineering, Wuhan Polytechnic University, Wuhan 430023, China; wz45151204@163.com (Z.W.); hujie9231@126.com (J.H.); zhanglei@whpu.edu.cn (L.Z.); m17663252107@163.com (Z.Z.); 18883632995@163.com (H.L.); yongzhang@whpu.edu.cn (Y.Z.); fgzcch@whpu.edu.cn (G.F.)
* Correspondence: xubing200806@163.com

Abstract: A novel Mn/TiO₂ catalyst, prepared through modification with the rare-earth metal Dy, has been employed for low-temperature selective catalytic reduction (SCR) denitrification. Anatase TiO₂, with its large specific surface area, serves as the carrier. The active component MnO_x on the TiO₂ carrier is modified using Dy. Dy_xMn/TiO_2, prepared via the impregnation method, exhibited remarkable catalytic performance in the SCR of NO with NH₃ as the reducing agent at low temperatures. Experiments and characterization revealed that the introduction of a suitable amount of the rare-earth metal Dy can effectively enhance the catalyst's specific surface area and the gas–solid contact area in catalytic reactions. It also significantly increases the concentration of Mn^{4+}, chemisorbed oxygen, and weak acid sites on the catalyst surface. This leads to a notable improvement in the reduction performance of the DyMn/TiO₂ catalyst, ultimately contributing to the improvement of the NH₃-SCR denitrification performance at low temperatures. At 100 °C and a space velocity of 24,000 h^{-1}, the $Dy_{0.1}Mn/TiO_2$ catalyst can achieve a 98% conversion rate of NO_x. Furthermore, its active temperature point decreases by 60 °C after the modification, highlighting exceptional catalytic efficacy at low temperatures. By doubling the space velocity, the NO_x conversion rate of the catalyst can still reach 96% at 130 °C, indicating significant operational flexibility. The selectivity of N₂ remained stable at over 95% before reaching 240 °C.

Keywords: NH₃-SCR de-NO_x; Dy; Mn/TiO₂ catalyst; low-temperature catalysis

1. Introduction

Due to the swift advancement of the industrial economy, the issue of environmental pollution has become progressively more pronounced and has gradually garnered widespread concern within society [1–3]. Nitrogen oxides (primarily NO), as a crucial air pollutant, significantly affect the chemical composition of the troposphere and are responsible for producing well-known phenomena such as the greenhouse effect, acid rain, PM2.5, and photochemical smog [4–9]. As a result, the emission of nitrogen oxides has garnered widespread concern. Countries worldwide have successively established stringent emission standards for nitrogen oxides in response to air pollution. Strict rules and regulations promote the rapid development of technology for treating NO_x [10–15].

Currently, there are three primary methods of controlling nitrogen oxides, which include raw material control technology prior to combustion, combustion process control technology, and post-combustion control technology. Currently, the initial two techniques can effectively decrease the overall volume of nitrogen oxides, yet meeting the rigorous emission norms proves to be a challenge. The post-combustion control technology has emerged as the cornerstone for complying with emission standards [16–20]. Currently, the most feasible methods for reducing NO_x emissions primarily involve selective non-catalytic reduction (SNCR) and selective catalytic reduction (SCR). Of these, selective catalytic

reduction of NO_x using ammonia as the reductant (NH_3-SCR) is the most widely used and effective technology in the flue gas denitrification industry. Currently, the V_2O_5-WO_3/TiO_2 catalyst, the most frequently employed in NH_3-SCR technology, exhibits outstanding denitrification performance within the temperature range of 280 °C to 400 °C. However, V_2O_5-WO_3/TiO_2 catalysts have activity at high temperatures and a narrow temperature window. According to the characteristics of high flue gas and sulfur content, the catalyst is prone to poisoning failure and high denitration cost [21–26]. The V_2O_5 contained in the spent catalyst after use exhibits biological toxicity, posing a threat to both the ecological environment and human health. Regulations have been issued by various countries globally to dispose of invalid V_2O_5-WO_3/TiO_2 catalysts as hazardous wastes, resulting in increased disposal costs. Therefore, the development of new low-temperature and harmless catalysts provides the NH_3-SCR process with advantages such as low energy consumption, low investment cost, and long catalyst life. Simultaneously, it is imperative that the non-toxic nature of the failed catalyst toward the environment is emphasized [27–37].

Zhang et al. [17] successfully prepared Cu-SAPO-34 and Mn/SAPO-34 catalysts through hydrothermal synthesis. Through the study of the low-temperature NH_3-SCR denitrification activity of the two catalysts, it was discovered that Mn had a more significant role in enhancing the catalyst's activity at low temperatures. The analysis of characterization revealed that MnO_2 exhibits a remarkable catalytic function in the oxidation of NO, thereby significantly enhancing the rapid progress of the SCR reaction.

In their study, Qi et al. [31] examined the SCR reaction mechanism of the MnO_x-CeO_2 catalyst system, which contains rare-earth elements, at low temperatures. The findings revealed that NH_3, when adsorbed on the Lewis acid sites on the catalyst surface, reacts with gaseous NO upon activation, resulting in the conversion of all intermediate products to NH_2NO, which subsequently decomposes to produce N_2 and water. Among them, Ce possesses a specific alkalinity, which facilitates the interaction of oxygen ions in the surrounding environment with NO_x, thereby oxidizing NO_x.

Niu et al. [38] were the first to modify Mn/TiO_2 with Tm, leading to a significant enhancement of the catalyst's selective catalytic activity at low temperatures. Upon addition of an appropriate amount of Tm, it was discovered that the concentration of Mn^{4+} on the catalyst's surface, the chemisorption of oxygen, NO, and NH_3, as well as the reduction performance of the Tm-Mn/TiO_2 catalyst, were significantly improved. This enhancement is beneficial for improving the NH_3-SCR reaction's effectiveness on NO_x.

To enhance the study of NO_x conversion activity at low temperatures, identify additional elements that can modify the catalyst, boost the selectivity for industrial application, and reduce the cost of implementation, our group has conducted extensive research on the modification of the conventional V_2O_5-WO_3/TiO_2 catalyst system, including the modification of transition metals such as copper, cadmium, and iron. The findings revealed that the reactive temperatures for the catalytic reactions were all above 240 °C, which is unsatisfactory for the current industrial optimization objectives. Therefore, we continue to choose the Mn/TiO_2 catalytic system for doping modification and utilize Dy from the rare-earth elements as the modifying element to enhance the conversion rate of NO at low temperatures. The results indicate that the inclusion of an adequate quantity of Dy can considerably enhance the conversion activity of Mn/TiO_2 to NO via NH_3-SCR technology, specifically at low temperatures ranging from 100 °C to 180 °C.

Rare-earth metals are primarily used as raw materials for rare-earth permanent magnet materials, making them one of the most significant applications of these metals. Rare-earth metals are extensively utilized in new energy batteries. In recent years, the field of denitration catalysts has gradually incorporated the rare-earth metals Tm and Ce, resulting in impressive research outcomes. In our research group, Dy was tasked with modifying the Mn/TiO_2 catalytic system. The prepared DyMn/TiO_2 catalyst exhibited outstanding catalytic performance at space velocities of 24,000 and 48,000 h^{-1} below 180 °C; this will greatly reduce the operating cost of SCR denitration. By successfully modifying the MnO_x/TiO_2 catalyst with dysprosium, the application scope of rare-earth resources can

be expanded. Additionally, these findings will serve as a valuable guide and reference for the widespread adoption of low-temperature catalysts in industrial SCR denitrification processes.

2. Results and Discussion

2.1. SCR Performance

Figure 1 shows the SCR performance test curve of the catalyst sample. At a space velocity of 24,000 h^{-1}, Figure 1a illustrates the variation of NO$_x$ conversion for Dy$_x$Mn/TiO$_2$ catalysts with varying molar ratios. Figure 1a reveals that all catalysts exhibit a tendency to initially rise and then decline within the temperature range of 70–340 °C. At 160 °C, the Mn/Ti catalyst achieved a 98% conversion of NO$_x$. After the introduction of the rare-earth metal Dy, the NO$_x$ conversion of the Dy$_x$Mn/TiO$_2$ catalyst improved significantly below 160 °C, demonstrating outstanding low-temperature catalytic activity. The conversion of NO$_x$ for the Dy$_{0.05}$Mn/TiO$_2$ and Dy$_{0.15}$Mn/TiO$_2$ catalysts reached 98% at 130 °C, while the Dy$_{0.1}$Mn/TiO$_2$ catalyst even achieved a 98% NO$_x$ conversion at 100 °C. Additionally, the activity temperature point decreased by 60 °C compared to its pre-modification state, demonstrating outstanding catalytic performance at low temperatures. At a space velocity of 48,000 h^{-1}, Figure 1b illustrates the variation of NO$_x$ conversion for Dy$_x$Mn/TiO$_2$ catalysts with varying molar ratios. Upon examination of Figure 1b, it is apparent that the catalytic capacity of all catalysts has diminished. However, the NO$_x$ conversion efficiency of the Dy$_{0.1}$Mn/TiO$_2$ catalyst surpasses that of other catalysts, attaining a remarkable 96% at 130 °C. The results indicate that the introduction of the rare-earth metal Dy can significantly enhance the NO$_x$ conversion of the Mn/Ti catalyst, and when the molar ratio of Dy/Ti is 0.1, the catalyst exhibits outstanding denitration performance.

Simultaneously, the series of prepared catalysts demonstrate notable catalytic activity within the Space velocity range of 24,000 h^{-1} to 48,000 h^{-1}, indicating their broad operational flexibility in catalytic reactions and making them highly suitable for industrial application. Figure 1c,d display the N$_2$ selectivity of Dy$_x$Mn/TiO$_2$ catalyst samples when the space velocity is 24,000 h^{-1} and 48,000 h^{-1}, respectively, ensuring an N$_2$ selectivity of over 95% below 240 °C. At elevated space velocities, when the temperature exceeds 260 °C, the selectivity decreases due to an increased likelihood of side reactions and a reduced contact time and chance between gas and catalyst, primarily attributed to the excessive space velocity. In summary, when the molar ratio of Dy/Ti is 0.1, the Dy$_x$Mn/TiO$_2$ catalyst sample exhibits the best low-temperature SCR denitrification performance and outstanding N$_2$ selectivity. Lastly, the stability of the Dy$_{0.1}$Mn/TiO$_2$ catalyst sample was tested at 150 °C. As shown in Figure 1e, the catalytic efficiency of the Dy$_{0.1}$Mn/TiO$_2$ catalyst sample consistently remained above 98% throughout the entire test period, demonstrating the catalyst's exceptional stability.

2.2. SEM, Crystallinity, and Porous Property Analyses

Figure 2 displays the SEM images of the Mn/TiO$_2$ catalyst and the Dy$_x$Mn/TiO$_2$ catalyst. As the molar ratio of Dy increases, the active components on the catalyst surface gradually increase, as evident from Figure 2. However, the surface of the Dy$_{0.15}$Mn/TiO$_2$ catalyst exhibited noticeable agglomeration, leading to a decrease in the catalyst's specific surface area. Concurrently, this phenomenon obscured the active sites on the surface to some extent, ultimately diminishing the catalyst's SCR catalytic activity. As shown in Figure 2c, the Dy$_{0.1}$Mn/TiO$_2$ catalyst boasts a considerable amount of active components uniformly distributed across its surface, thereby manifesting commendable catalytic activity in SCR catalytic performance experiments.

Figure 3 displays the XRD patterns of the Dy$_x$Mn/TiO$_2$ catalyst. All catalysts exhibited comparable XRD diffraction peaks, suggesting that the addition of the rare-earth metal Dy did not alter the crystal structure of the catalyst. Characteristic peaks of anatase TiO$_2$ were observed at 25.8°, 38.0°, 47.6°, 54.5°, 62.8°, 69.5°, and 75.2°. Anatase TiO$_2$ is more beneficial for enhancing the catalytic performance of SCR [35]. As shown in Figure 3, no characteristic

peaks of Mn and Dy oxides were observed on the surface of the catalyst sample. This suggests that the oxides of Mn and Dy are either highly dispersed on the surface of the catalyst or exist in an amorphous form, which cannot be detected by XRD [39]. Upon the introduction of the rare-earth metal Dy, as the Dy/Ti molar ratio increases, the diffraction peak intensity exhibits a trend of initial decrease, subsequent increase, and subsequent decrease. The introduction of Dy into the system indicates a reduction in the crystallinity of the TiO$_2$ support. Table 1 presents the ICP–OES analysis of catalysts. The results indicate that the actual loading mass of Dy in each catalyst essentially aligns with the theoretical value. It also demonstrates that the prepared catalyst does indeed contain a specific amount of Mn and Dy oxides, which to some extent corroborates the XRD data analysis.
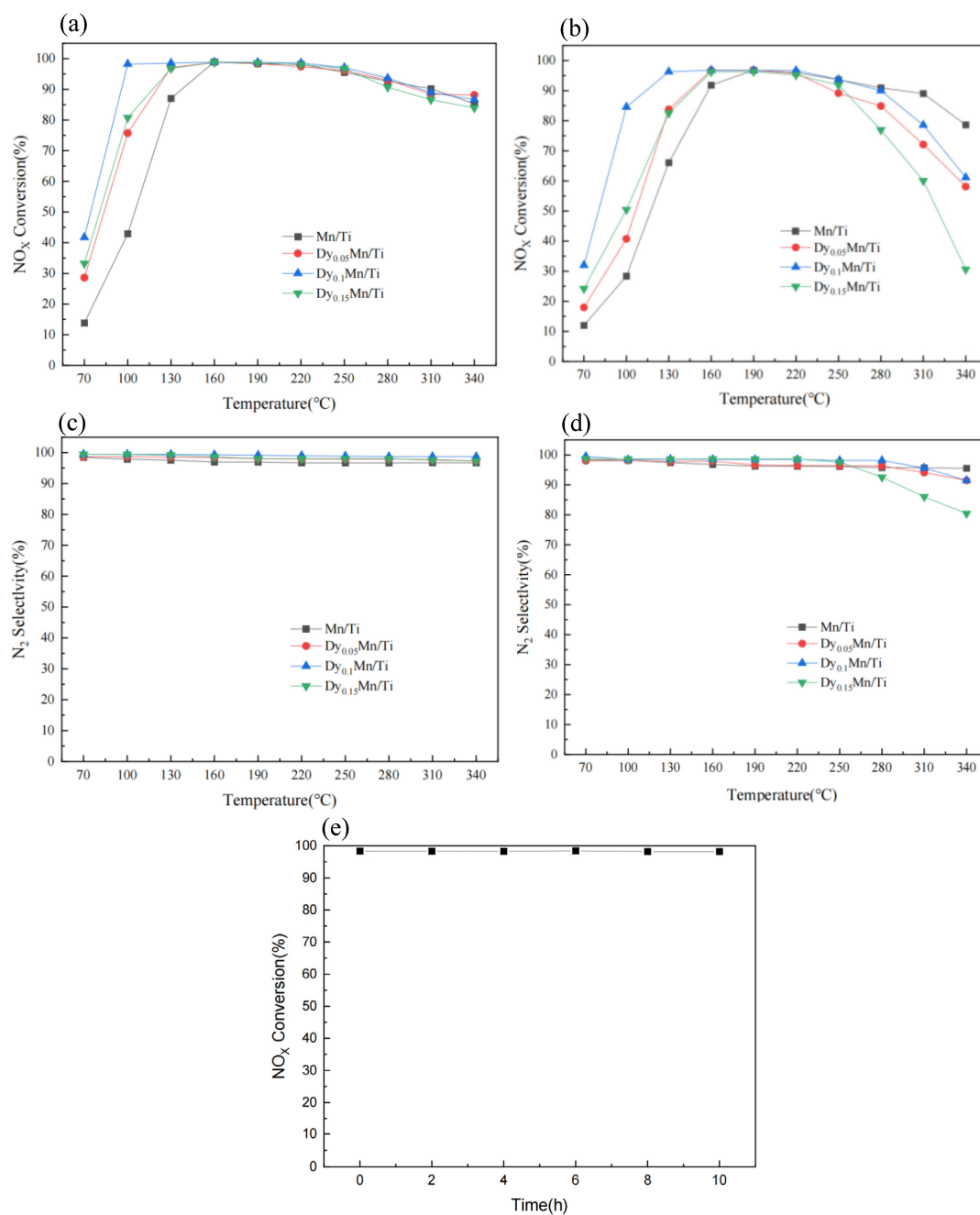

Figure 1. Effect of Dy/Mn molar ratio on NO$_x$ conversion (**a**,**b**) and N$_2$ selectivity at different space velocities (24,000 h^{-1}, 48,000 h^{-1}) (**c**,**d**); results of Dy$_{0.1}$Mn/TiO$_2$ catalyst stability testing (**e**).
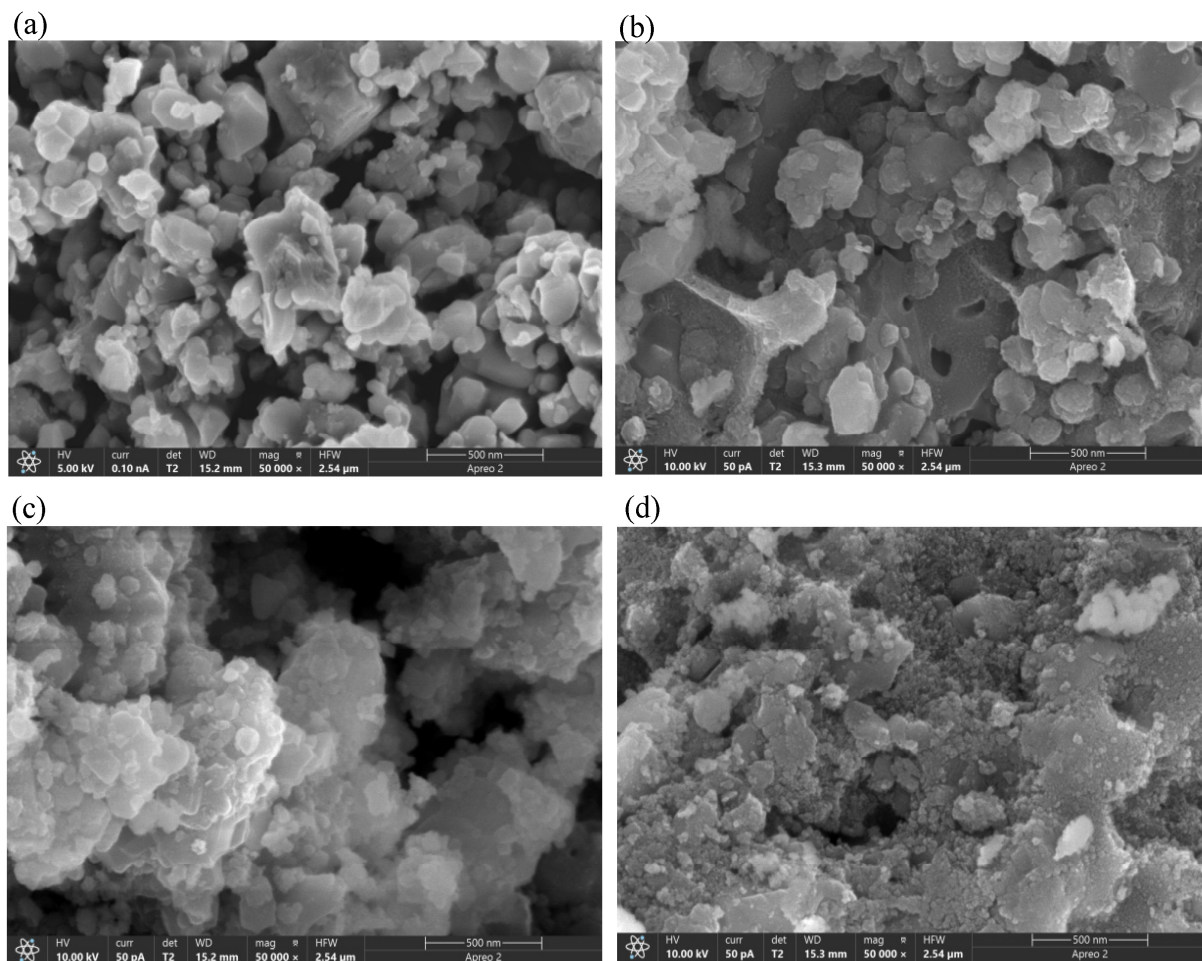
Figure 2. SEM microstructures of the different catalysts. (**a**) Surface morphology of Mn/TiO_2. (**b**) Surface morphology of $Dy_{0.5}Mn/TiO_2$. (**c**) Surface morphology of $Dy_{0.1}Mn/TiO_2$. (**d**) Surface morphology of $Dy_{0.15}Mn/TiO_2$.
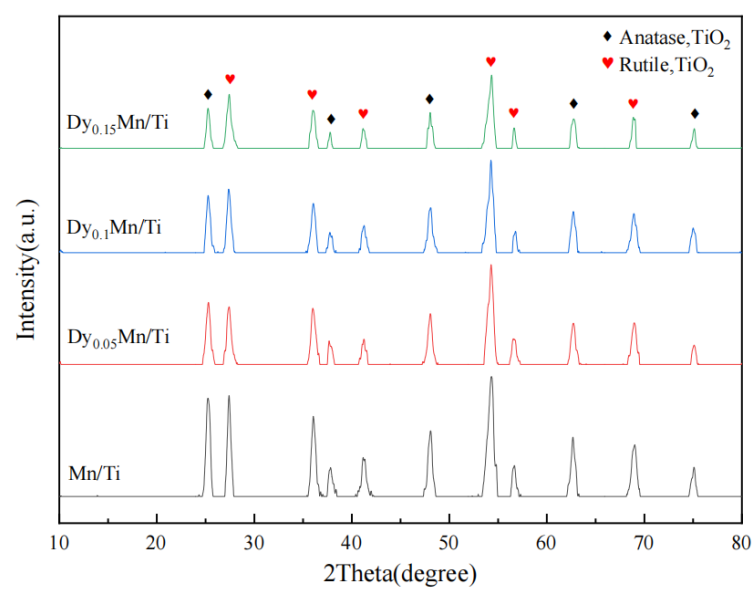

Figure 3. XRD patterns of the different catalysts.

Table 1. Mass fraction of the Dy_xMn/TiO_2 catalysts measured with ICP–OES.

Catalyst Sample	Theoretical Load Capacity	Actual Load Capacity
Mn/TiO_2	15.55% Mn	14.41% Mn
$Dy_{0.05}Mn/TiO_2$	14.29% Mn, 7.03% Dy	13.07% Mn, 6.70% Dy
$Dy_{0.1}Mn/TiO_2$	13.22% Mn, 13.02% Dy	12.18% Mn, 13.20% Dy
$Dy_{0.15}Mn/TiO_2$	12.30% Mn 18.18% Dy	13.02% Mn, 18.85% Dy

　　　　Figure 4 depicts the adsorption–desorption isotherms of all catalysts. The catalysts exhibit type IV isotherms and type H2 hysteresis loops, which are hallmarks of mesoporous materials. The measurement and calculation of specific surface area, pore volume, and pore diameter are based on BET and BJH equations, as detailed in Table 2 below. The specific surface area of the Mn/TiO_2 catalyst is only 7.94 m^2/g. With the introduction of Dy, the specific surface area initially increases and then decreases. The pore volume becomes larger but the pore size becomes smaller. The specific surface area of the $Dy_{0.1}Mn/TiO_2$ catalyst is as high as 49.47 m^2/g, which is higher than 37.01 m^2/g in the literature [39]. The large surface area of the catalyst facilitates the rapid adsorption of reactants and the desorption of products on the catalyst surface, thereby enhancing the low-temperature SCR catalytic performance of the catalyst [38]. The results indicate that the specific surface area of the catalyst and the gas–solid contact area of the catalytic reaction can be significantly increased when an appropriate amount of the rare-earth metal Dy is introduced, which also enhances the SCR denitrification activity of the catalyst.
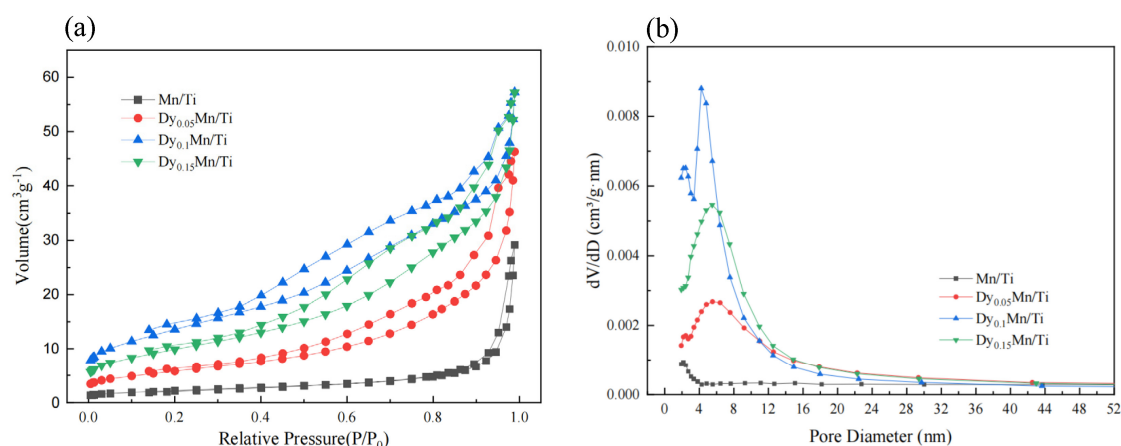

Figure 4. (**a**) Nitrogen adsorption-esorption curve of the different catalysts. (**b**) Pore size distribution curve of the different catalysts.

Table 2. The pore analysis data of the different catalysts.

Catalyst Sample	BET Surface Area (m^2/g)	Pore Volume (cm^3/g)	Average Pore Diameter (nm)
Mn/TiO_2	7.94	0.044	26.78
$Dy_{0.05}Mn/TiO_2$	21.00	0.071	13.62
$Dy_{0.1}Mn/TiO_2$	49.47	0.086	7.53
$Dy_{0.15}Mn/TiO_2$	35.91	0.087	9.88

2.3. XPS Analysis

　　　　Figure 5 displays the X-ray photoelectron spectroscopy (XPS) characterization of the Dy_xMn/TiO_2 catalyst, aiming to investigate the variations in elemental valence on the surface of various catalysts. It involves the separation and fitting of characteristic peaks for Mn, O, and Dy elements in each catalyst, and the computation of the relative concentrations of Mn, O, and Dy elements in varying valence states on the surface of each catalyst. As

illustrated in Figure 5a, the photoelectron peaks for Mn 2p3/2 and Mn 2p1/2 are situated around 642.0 eV and 653.5 eV, respectively. Mn 2p3/2 was categorized into three electronic peaks, namely Mn^{2+} (641.2 ± 0.1 eV), Mn^{3+} (642.3 ± 0.1 eV), and Mn^{4+} (643.8 ± 0.1 eV) [38]. According to relevant literature [39], high levels of Mn^{4+} promote the NH_3-SCR catalytic reduction reaction. Table 2 shows that with the addition of the rare-earth metal Dy, the $Mn^{4+}/(Mn^{2+} + Mn^{3+} + Mn^{4+})$ ratio first increases and then decreases. The $Dy_{0.1}Mn/TiO_2$ catalyst exhibits the highest ratio, aligning with the results of the SCR performance test. This aligns with the literature's conclusion: Mn^{4+} concentration is a crucial factor in determining the catalyst's low-temperature catalytic activity.
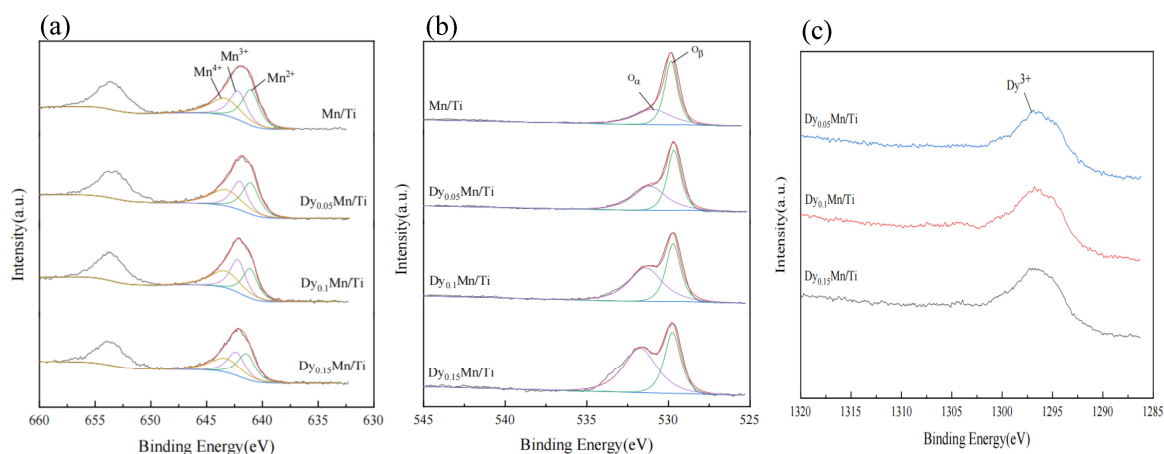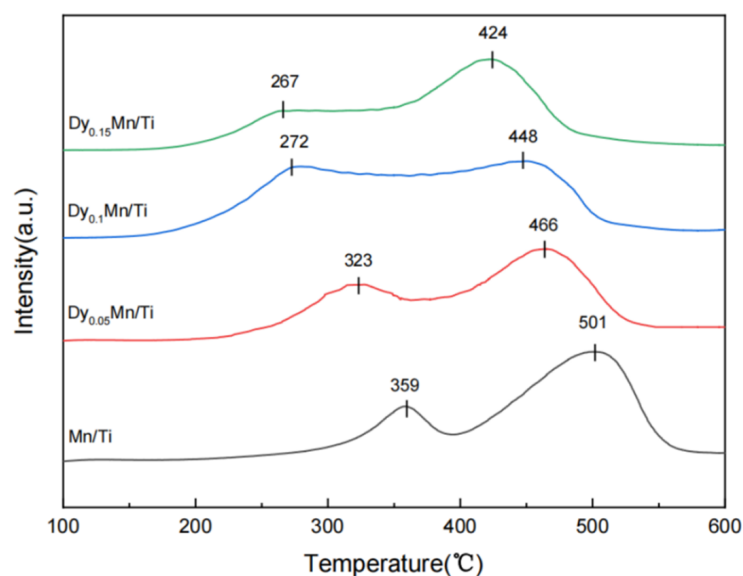

Figure 5. XPS of the different catalysts: (**a**) Mn 2p, (**b**) O 1s, (**c**) Dy 4d.

As shown in Figure 5b, all catalysts exhibit two overlapping peaks around 529.8 eV and 531.5 eV [38]. The peak at 529.8 eV belongs to lattice oxygen (denoted as O_β), while the peak at 531.5 eV belongs to adsorbed oxygen (denoted as O_α). According to a literature report [39], O_α has a higher mobility than O_β. It can be converted to lattice oxygen at oxygen vacancies on the catalyst surface, thereby enhancing the oxidation ability of NO at low temperatures and promoting the rapid progress of the SCR reaction. Table 2 reveals that with the addition of the rare-earth metal Dy, the ratio of $O_\alpha/(O_\alpha + O_\beta)$ on the catalyst surface gradually increases. This suggests that the amount of adsorbed oxygen is a pivotal factor influencing the catalyst's low-temperature catalytic performance. The location of Dy 4d is indicated to be around 1294 eV, as depicted in Figure 5c, which corresponds to the Dy^{3+} on the catalyst surface.

2.4. H_2-TPR, NH_3-TPD Analysis

The H_2-TPR experiment is conducted to investigate the redox behavior of the Dy_xMn/TiO_2 catalyst. The redox properties of catalysts significantly determine their catalytic properties. As illustrated in Figure 6, all catalysts exhibit two broad, overlapping reduction peaks within the temperature range of 150–550 °C. For the Mn/Ti catalyst, the reduction peak around 359 °C is attributed to the reduction process of $MnO_2 \rightarrow Mn_2O_3$ [31,38]. The reduction peak within the temperature range of 420–520 °C is attributed to the reduction process of $Mn_2O_3 \rightarrow Mn_3O_4 \rightarrow MnO$ [39]. Compared to the peak of Mn/TiO_2, the reduction peak of the Dy–Mn/Ti catalyst shifted towards lower temperatures due to the synergistic effect between Dy and Mn/TiO_2. Among them, the $Dy_{0.1}Mn/TiO_2$ catalyst and the $Dy_{0.15}Mn/TiO_2$ catalyst exhibit the lowest reduction peak temperatures. The peak performance of the $Dy_{0.1}Mn/TiO_2$ catalyst is notably broader and encompasses regions of lower temperature. Upon calculating the peak area, it is observed that the $Dy_{0.1}Mn/TiO_2$ catalyst boasts the largest peak area, as illustrated in Table 3. The H_2-TPR results indicate that the $Dy_{0.1}Mn/TiO_2$ catalyst exhibits the optimal reduction behavior at low temperatures

and demonstrates the highest catalytic activity among the SCR catalysts, corroborating the findings from the prior SCR catalytic performance tests.

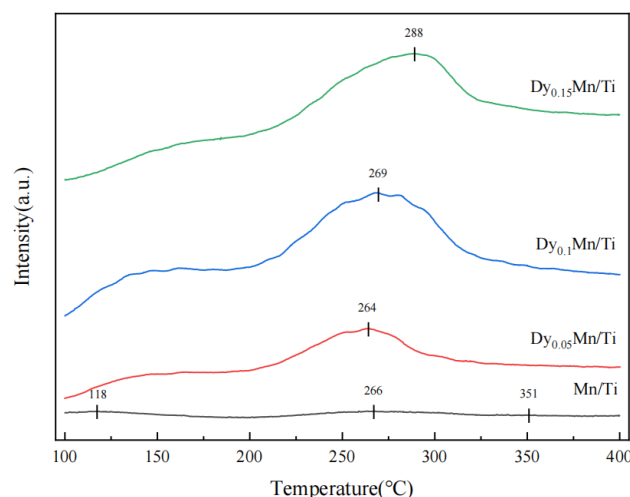**Figure 6.** H_2-TPR analysis of the different catalysts.

Table 3. The valence concentration of elements on the surface of the different catalysts and H_2 reduction peak area.

Catalyst Sample	Mn^{4+}/Mn^{n+}(%)	$O_\alpha/(O_\alpha + O_\beta)$ (%)	H_2 Reduction Peak Area (%)	NH_3-TPD Peak Area (%)
Mn/TiO_2	31.75	39.59	76.91	7.28
$Dy_{0.05}Mn/TiO_2$	33.64	49.36	73.29	44.37
$Dy_{0.1}Mn/TiO_2$	35.06	60.21	100.00	100.00
$Dy_{0.15}Mn/TiO_2$	33.02	61.32	77.64	78.88

Note: The peak area of H_2 reduction and NH_3-TPD are normalized with $Dy_{0.1}Mn/TiO_2$ as the standard.

In the NH_3-SCR reaction, the adsorption capacity of the catalyst for NH_3 is crucial. Figure 7 shows the NH_3-TPD characterization results for all Dy_xMn/TiO_2 catalysts. Three weak desorption peaks can be observed for the Mn/TiO_2 catalyst. The peak around 118 °C is attributed to the physical adsorption of NH_3 on the catalyst, the peak around 266 °C is attributed to the desorption peak of NH_3 adsorbed on the Bronsted acid site (weak acid), and the peak around 351 °C is attributed to the desorption peak of NH_3 adsorbed on the Lewis acid site (strong acid) [38]. Upon introduction of the rare-earth metal Dy, the desorption peak on weak acid significantly intensified. As the Dy content increased, the area of the desorption peak initially expanded and then diminished. As illustrated in Table 3, it is observed that the peak area of NH_3 desorption for the $Dy_{0.1}Mn/TiO_2$ catalyst is the largest among all catalysts, suggesting the highest number of weak acid sites on the catalyst surface. According to literature reports [38], weak acids are crucial to the low-temperature catalytic activity of catalysts. Consequently, the moderate incorporation of Dy notably enhances the adsorption capacity of NH_3 on the catalyst surface, substantially increases the number of weak acid sites on the catalyst surface, and consequently boosts the catalyst's activity at low temperatures. The results of the NH_3-TPD characterization experiments further corroborate and validate the previous results of the NH_3-SCR performance tests.

Figure 7. NH_3-TPD analysis of the different catalysts.

3. Experiment

3.1. Synthesis Catalyst

A series of $DyMn/TiO_2$ catalysts with varying Dy/Mn molar ratios were prepared using the impregnation method. The detailed synthesis procedure is as follows: Weigh an appropriate amount of Dysprosium Nitrate (AR, purchased from Shanghai Mcleam Biochemical Technology Co., Ltd., Shanghai, China) and manganese acetate (AR, purchased from Alddin Reagent Co., Ltd., Shanghai, China) into a beaker that holds 50 mL of deionized water. To facilitate dissolution, place the beaker into a magnetic water bath stirring pot and stir thoroughly. Weigh an appropriate amount of titanium dioxide powder (AR, purchased from Sinopharm Chemical Reagent Co., Ltd., Shanghai, China) and add it gradually to the beaker. Stir at room temperature for 2 h, and then raise the temperature to 90 °C using the water bath. Continue stirring until the water evaporates to a viscous state. Then, remove the beaker and dry it in a 110 °C drying oven for 15 h to obtain a dry, block-like solid. Subsequently, transfer the block-shaped solid to a quartz crucible and roast it in a muffle furnace at 400 °C (with a heating rate of 6 °C/min) for four hours in an air atmosphere to yield the calcined solid particles. Finally, make a catalyst powder with a particle diameter ranging from 0.25 to 0.45 mm through tablet pressing, grinding, and sieving to achieve a mesh size of 40–60. The synthesized catalyst series is denoted by the symbol Dy_xMn/TiO_2, where x represents the molar ratio of Dy to Ti (Mn:Ti = 0.3:1; the mass fraction of Dy was 7.02%, 13%, and 18.13%, respectively). Additionally, when x is 0, it corresponds to the Mn/TiO_2 catalyst, also prepared via the impregnation method. The reaction mechanism is shown in Figure 8.
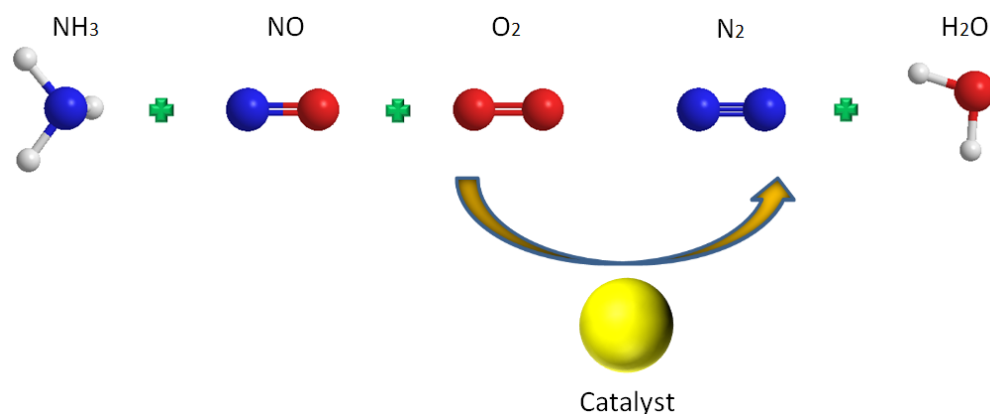
Figure 8. Main schematic diagram of NH_3-SCR denitration.

3.2. Characterization of Catalysts

The phase composition and crystal phase composition of the catalyst were analyzed using an X-ray diffractometer (D8ADVANCE, Bruker Corporation, Bremen, Germany), with cu-k α serving as the radiation source. The tube voltage was set to 40 kV, the tube current to 30 mA, the XRD scanning range to 10–80°, and the step size to 0.02°. A scanning electron microscope (JSM-7610FPlus, JEOL Co., Ltd., Tokyo, Japan) was used to observe the morphology of aerogel under an accelerating voltage of 15 kV. The specific surface area and pore structure of the samples were determined using a specific surface area and pore volume aperture analyzer (ASAP2460, Micromeritics, Norcross, GA, USA). The calculation of test data was performed according to BET analysis. The X-ray photoelectron spectrometer (Escalab 250xi, Thermo Fisher Scientific, Waltham, MA, USA) was employed for the XPS test, with the aim of investigating the valence state of atoms present on the surface of the catalyst. The binding energies of the measured elements were corrected using the C 1s peak (284.6 eV). An analysis was conducted using an Al Kα X-ray with a tube voltage of 1486.6 eV. The content of metal elements in the catalyst was determined by inductively coupled plasma atomic emission spectrometry (ICPOES 730, Aglient Technology Co., Ltd., Santa Clara, CA, USA).

The H_2-TPR experiment employed the BELCAT-A system (BELCAT-A, Bayer, Tokyo, Japan) for temperature-programmed reduction, aimed at examining the impact of the catalyst's redox property on its catalytic performance. Test procedure: Weigh 100 mg of sample and transfer it into a reaction tube. Dry it at a rate of 10 °C/min, increasing from room temperature to 300 °C. Use a high-purity nitrogen flow rate (30 mL/min) to purge it for 1 h, and then allow it to cool down to 50 °C. Convert N_2 to a reducing gas (10% H_2/N_2) for purge purposes, remove any residual N_2 on the sample surface and within the pipeline, maintaining a flow rate of 30 mL/min, then increase the temperature from 50 °C to 700 °C at a rate of 10 °C/min. Record the TCD signal value.

The NH_3-TPD analysis was also conducted using the BELCAT-A system (BELCAT-A, Bayer, Japan) to investigate the impact of acidity on the catalytic performance of the catalyst. Test procedure: Weigh 50–200 mg of sample and transfer it into a reaction tube. Program the temperature to rise to 300 °C at a rate of 10 °C/min for drying pretreatment. Purge it with a N_2 flow of 30 mL/min for 1 h and cool it to 50 °C. Subsequently, introduce a 10% NH_3/N_2 mixture (30 mL/min) and leave it to saturate for an hour. Afterward, switch on the flow of N_2 (30 mL/min) to purge for an hour and remove any weakly physically adsorbed NH_3 on the surface. Finally, under an N_2 atmosphere, raise the temperature at a rate of 10 °C/minute until it reaches 600 °C for desorption. The desorbed gas is detected using a thermal conductivity detector (TCD).

3.3. Characterization of Catalysts

The laboratory self-made denitration activity evaluation equipment is the experimental device employed for the NH_3-SCR performance test of the experimental catalyst (Figure 9). The reactor has an inner diameter of 1 cm and a length of 50 cm. The center of the reaction tube is filled with 0.096 g of catalyst, and the temperature of the reactor is monitored using a thermocouple. During the reaction process, the temperature is maintained between 100–400 °C. For every 30 °C increase, the temperature is held for approximately 20 min to stabilize the concentration of each tail gas component. Real-time data are recorded sequentially. Rotor flowmeters and volume flowmeters are utilized to harmoniously regulate the flow of gases from each pathway, stabilizing the overall flow rate of the simulated flue gas atmosphere. Additionally, the gas volume space velocity is adjusted to 24,000 h^{-1} (Flow rate is 300 mL/min) and 48,000 h^{-1}, respectively. An online flue gas analyzer (GW-2000) is employed to monitor the NO_x content in the reactor's exhaust, a nitrous oxide detector (FGD2-C-N_2O) is utilized to measure the N_2O level in the reaction's

exhaust, and a specific length gas detection tube is used to determine the concentration of ammonia in both the intake air and the exhaust.

$$NO_x conversion\ (\%) = \frac{[NO_x]_{in} - [NO_x]_{out}}{[NO_x]_{in}} \times 100\% \tag{1}$$

$$N_2\ selectivity\ (\%) = \frac{[NO_x]_{in} + [NH_3]_{in} - [NO_x]_{out} - [NH_3]_{out} - [N_2O]_{out}}{[NO_x]_{in} + [NH_3]_{in} - [NO_x]_{out} - [NH_3]_{out}} \times 100\% \tag{2}$$
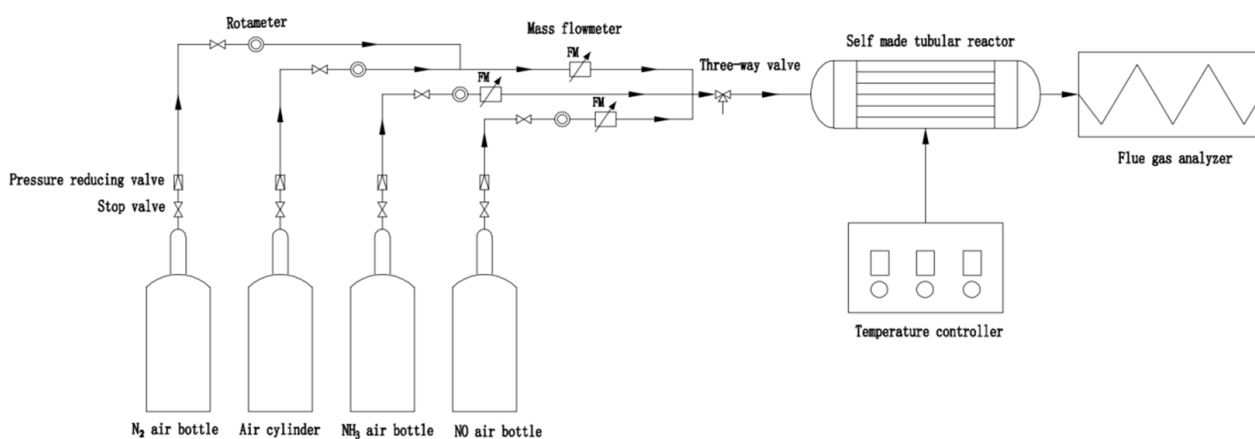

Figure 9. Flow chart of catalyst performance test device.

4. Conclusions

An efficient Mn/TiO_2 catalyst, prepared through modification with the rare-earth metal Dy, has been employed for low-temperature selective catalytic reduction (SCR) denitrification. The Dy_xMn/TiO_2 catalyst, prepared by the impregnation method, exhibited outstanding catalytic performance. Experiments and characterization revealed that the introduction of a suitable amount of the rare-earth metal Dy can effectively enhance the specific surface area of the catalyst and increase the contact area for gas–solid reactions. Concurrently, the incorporation of the rare-earth metal Dy significantly enhances the concentration of Mn^{4+} on the catalyst surface and the chemisorption of oxygen, significantly contributing to the improvement of the catalyst's activity. Lastly, the SCR catalytic performance was confirmed through NH_3-TPD and H_2-TPR experiments. The findings indicate that the incorporation of a suitable amount of the metal Dy significantly enhances the adsorption capacity of NH_3 on the catalyst surface and effectively augments the number of weak acid sites on the catalyst surface, thereby enhancing the catalyst's activity at low temperatures, ameliorating the reduction performance of the $DyMn/TiO_2$ catalyst, and ultimately bolstering the performance of NH_3-SCR denitration at low temperatures. The $Dy_{0.1}Mn/TiO_2$ catalyst can achieve a 98% NO_x conversion rate at 100 °C under a space velocity of 24,000 h^{-1}. Additionally, its active temperature point is 60 °C lower than before modification, demonstrating an outstanding catalytic performance at low temperatures. After doubling the space velocity, the NO_x conversion of the catalyst remains at 96% even at 130 °C, demonstrating substantial operational flexibility. The selectivity to N_2 remains above 95% up to 240 °C.

Author Contributions: Investigation: B.X., Z.W., J.H., L.Z., Z.Z., H.L., Y.Z. and G.F.; original manuscript writing: B.X. and Z.W.; manuscript review: B.X., J.H. and L.Z. All authors have read and agreed to the published version of the manuscript.

References

1. Li, Y.; Leng, X.; Ma, S.; Zhang, T.; Yuan, F.; Niu, X.; Zhu, Y. Effects of Mo addition on the NH_3-SCR of NO reaction over $Mo_a MnTi_{10}O_x$ (a = 0.2, 0.4, 0.6 and 0.8): Synergistic action between redox and acidity. *Catal. Today* **2020**, *339*, 254–264. [CrossRef]
2. Zhou, J.; Guo, R.; Zhang, X.; Liu, Y.; Pan, W. Cerium oxide—Based catalysts for low-temperature selective catalytic reduction of NO_x with NH_3: A review. *Energ. Fuel* **2021**, *35*, 2981–2998. [CrossRef]
3. Xie, H.; He, P.; Chen, C.; Yang, C.; Chai, S.; Wang, N.; Ge, C. Improvement of Sb-Modified Mn-Ce/TiO_2 Catalyst for SO_2 and H_2O Resistance at Low-Temperature SCR. *Catal. Lett.* **2023**, *153*, 2838–2852.
4. Jiang, H.; Wang, H.; Kuang, L.; Li, G.; Zhang, M. Synthesis of MnO_x–CeO_2·NO_x catalysts by polyvinyl pyrrolidone–assisted supercritical antisolvent precipitation. *J. Mater. Res.* **2014**, *29*, 2188–2197. [CrossRef]
5. Kapteijn, F.; Singoredjo, L.; Andreini, A.; Moulijn, J.A. Activity and selectivity of pure manganese oxides in the selective catalytic reduction of nitric oxide with ammonia. *Appl. Catal. B-Environ.* **1994**, *3*, 173–189. [CrossRef]
6. Dimitrios, K.P.; Pappas, A.; Thirupathi, B.; Punit, B.; Panagiotis, G.S. Novel manganese oxide confined interweaved titania nanotubes for the low-temperature Selective Catalytic Reduction (SCR) of NO_x by NH_3—ScienceDirect. *J. Catal.* **2016**, *334*, 1–13.
7. Yang, S.; Qi, F.; Liao, Y.; Xiong, S.; Lan, Y.; Shan, W.; Li, J. Dual effect of sulfation on the selective catalytic reduction of NO with NH_3 over MnO_x/TiO_2: Key factor of NH_3 distribution. *Ind. Eng. Chem. Res.* **2014**, *53*, 5810–5819. [CrossRef]
8. Yang, S.; Qi, F.; Xiong, S.; Dang, H.; Liao, Y.; Wong, P.; Li, J. MnO_x supported on Fe-Ti spinel: Anovel Mn based low temperature SCR catalyst with a high N_2 selectivity. *Appl. Catal. B.-Environ.* **2016**, *181*, 570–580. [CrossRef]
9. Zhang, B.; Zhang, S.; Liu, B. Comparative study on transition element doped Mn-Zr-Ti-oxides catalysts for the low-temperature selective catalytic reduction of NO with NH_3. *React. Kinet. Mech. Catal.* **2019**, *127*, 637–652. [CrossRef]
10. Zhang, B.; Liebau, M.; Suprun, W.; Liu, B.; Zhang, S.; Glaeser, R. Suppression of N_2O formation by H_2O and SO_2 in the selective catalytic reduction of NO with NH_3 over a Mn/Ti-Si catalyst. *Catal. Sci. Technol.* **2019**, *9*, 4759–4770. [CrossRef]
11. Qiu, L.; Wang, Y.; Pang, D.; Feng, O.; Zhang, C.; Cao, G. Characterization and catalytic activity of Mn–Co/TiO_2 catalysts for NO oxidation to NO_2 at low temperature. *Catalysis* **2016**, *6*, 9. [CrossRef]
12. Qiu, L.; Meng, J.; Pang, D.; Zhang, C.; Ouyang, F. Reaction and characterization of Co and Ce doped Mn/TiO_2 catalysts for low-temperature SCR of NO with NH_3. *Cawal. Lett.* **2015**, *145*, 1500–1509. [CrossRef]
13. Qiu, L.; Pang, D.; Zhang, C.; Meng, J.; Zhu, R.; Ouyang, F. In situ IR studies of Co and Ce doped Mn/TiO_2 catalyst for low-temperature selective catalytic reduction of NO with NH_3. *Appl. Surf. Sci.* **2015**, *357*, 189–196. [CrossRef]
14. Guan, B.; Zhan, R.; Lin, H.; Huang, Z. Review of State of the Art Technologies of Selective Catalytic Reduction of NO_x from Diesel Engine Exhaust. *Appl. Therm. Eng.* **2014**, *66*, 395–414. [CrossRef]
15. Liu, L.; Su, S.; Xu, K.; Li, H.; Qing, M.; Hu, S.; Wang, Y.; Xiang, J. Insights into the highly efficient Co modified MnSm/Ti catalyst for selective catalytic reduction of NO with NH_3 at low temperature. *Fuel* **2019**, *255*, 115798. [CrossRef]
16. De La Torre, U.; Pereda-Ayo, B.; González-Marcos, J.A.; Gutiérrez-Ortiz, M.A.; González-Velasco, J.R. Performance of Cu-ZSM-5 in a coupled monolith NSR-SCR system for NO_x removal in lean-burn engine exhaust. *Top. Catal.* **2016**, *59*, 259–267. [CrossRef]
17. Zhang, M.; Cao, H.; Chen, Y.; Jiang, H. Role of Mn: Promotion of fast-SCR for Cu-SAPO-34 in low-temperature selective catalytic reduction with ammonia. *Catal. Surv. Asia* **2019**, *23*, 245–255. [CrossRef]
18. Liu, X.; Zhao, Z.; Ning, R.; Qin, Y.; Zhu, T.; Liu, F. Ce-Doped V_2O_5-WO_3/TiO_2 with low vanadium loadings as SCR catalysts and the resistance of H_2O and SO_2. *Catal. Lett.* **2019**, *150*, 375–383. [CrossRef]
19. Gao, Y.; Jiang, W.; Luan, T.; Li, H.; Zhang, W.; Feng, W.; Jiang, H. High-efficiency catalytic conversion of NO_x by the synergy of nanocatalyst and plasma: Effect of Mn-based bimetallic active species. *Catalysts* **2019**, *9*, 103. [CrossRef]
20. Sun, P.; Guo, R.; Liu, S.; Wang, S.; Pan, W.; Li, M. The enhanced performance of MnO_x catalyst for NH_3-SCR reaction by the modification with Eu. *Appl. Catal. A-Gen.* **2017**, *531*, 129–138. [CrossRef]
21. Gao, F.; Tang, X.; Yi, H.; Li, J.; Zhao, S.; Wang, J.; Chu, C.; Li, C. Promotional mechanisms of activity and SO_2 tolerance of Co- or Ni-doped MnO_x-CeO_2 catalysts for SCR of NO_x with NH_3 at low temperature. *Chem. Eng. J.* **2017**, *317*, 20–31. [CrossRef]

22. Gao, Y.; Luan, T.; Zhang, M.; Zhang, W.; Feng, W. Structure-activity relationship study of Mn/Fe ratio effects on Mn-Fe-Ce-O$_{x/\gamma}$-Al$_2$O$_3$ nanocatalyst for NO oxidation and fast SCR reaction. *Catalysts* **2018**, *8*, 642. [CrossRef]

23. Liu, Z.; Chen, C.; Zhao, J.; Yang, L.; Sun, K.; Zeng, L.; Pan, Y.; Liu, Y.; Liu, C. Study on the NO$_2$ production pathways and the role of NO$_2$ in fast selective catalytic reduction DeNO$_x$ at low-temperature over MnO$_x$/TiO$_2$ catalyst. *Chem. Eng. J.* **2020**, *379*, 122288. [CrossRef]

24. Li, W.; Zhang, C.; Li, X.; Tan, P.; Zhou, A.; Fang, Q.; Chen, G. Ho-modified Mn-Ce/TiO$_2$ for low-temperature SCR of NO with NH$_3$: Evaluation and characterization. *Chin. J. Catal.* **2018**, *39*, 1653–1663. [CrossRef]

25. Zhang, T.; Ma, S.; Chen, L.; Li, R.; Leng, X.; Li, Y.; Yuan, F.; Niu, X.; Zhu, Y. Effect of Cu doping on the SCR activity over the CumCe$_{0.1-m}$TiO$_x$ (m = 0.01, 0.02 and 0.03) catalysts. *Appl. Catal. A-Gen.* **2019**, *570*, 251–261. [CrossRef]

26. Wang, S.; Guo, R.; Pan, W.; Li, M.; Sun, P.; Liu, S.; Liu, S.; Sun, X.; Liu, J. The deactivation mechanism of Pb on the Ce/TiO$_2$ catalyst for the selective catalytic reduction of NO$_x$ with NH$_3$: TPD and DRIFT studies. *Phys. Chem. Chem. Phys.* **2017**, *19*, 5333–5342. [CrossRef] [PubMed]

27. Yu, Z.; Xu, L.; Liang, Z.; Wang, Z. Doping and immobilization of TiO$_2$ with element Na and raschig rings. *Chem. Phys. Lett.* **2019**, *732*, 136634.

28. Fan, Z.; Shi, J.; Gao, C.; Gao, G.; Wang, B.; Wang, Y.; He, C.; Niu, C. Gd-modified MnO$_x$ for the selective catalytic reduction of NO by NH$_3$: The promoting effect of Gd on the catalytic performance and sulfuresistance. *Chem. Eng. J.* **2018**, *348*, 820–830. [CrossRef]

29. Xu, Q.; Su, R.; Cao, L.; Li, Y.; Yang, C.; Luo, Y.; Street, J.; Jiao, P.; Cai, L. Facile preparation of high-performance Fe-doped Ce-Mn/TiO$_2$ catalysts for the low-temperature selective catalytic reduction of NO$_x$ with NH$_3$. *RSC Adv.* **2017**, *7*, 48785–48792. [CrossRef]

30. Li, Y.; Li, Y.; Shi, Q.; Qiu, M.; Zhan, S. Novel hollow microspheres Mnx Co$_{3-x}$ O$_4$ (x = 1, 2) with remarkable performance for low-temperature selective catalytic reduction of NO with NH$_3$. *J. Sol.-Gel. Sci. Technol.* **2017**, *81*, 576–585. [CrossRef]

31. Qi, G.; Yang, R.T.; Chang, R. MnO$_x$—CeO$_2$ mixed oxides prepared by co-precipitation for selective catalytic reduction of NO with NH$_3$ at low temperatures. *Appl. Catal. B-Environ.* **2004**, *51*, 93–106. [CrossRef]

32. Tang, X.; Hao, J.; Yi, H.; Li, J. Low Temperature SCR of NO with NH$_3$ over AC/C supported manganese-based monolithic catalysts. *Catal. Today* **2007**, *126*, 406–411. [CrossRef]

33. Cheng, K.; Liu, J.; Zhang, T.; Li, J.; Duan, A. Effect of Ce doping of TiO$_2$ support on NH$_3$–SCR activity over V$_2$O$_5$-WO$_3$/CeO$_2$-TiO$_2$ catalyst. *J. Environ. Sci.* **2014**, *26*, 2106–2113. [CrossRef]

34. Jing, W.; Guo, Q.; Hou, Y.; Ma, G.; Han, X.; Huang, Z. Catalytic role of vanadium(V) sulfate on activated Carbon for SO$_2$ oxidation and NH$_3$–SCR of NO at low temperatures. *Catal. Commun.* **2014**, *56*, 23–26. [CrossRef]

35. Liu, Z.; Zhang, S.; Li, J.; Zhu, J.; Ma, L. Novel V$_2$O$_5$–CeO$_2$/TiO$_2$ catalyst with low vanadium loading for the selective catalytic reduction of NO$_x$ by NH$_3$. *Appl. Catal. B-Environ.* **2014**, *158–159*, 11–19. [CrossRef]

36. Yang, S.; Xiong, S.; Liao, Y.; Xiao, X.; Qi, F.; Peng, Y.; Fu, Y.; Shan, W.; Li, J. Mechanism of N$_2$O Formation during the Low–Temperature Selective Catalytic Reduction of NO with NH$_3$ over Mn-Fe Spinel. *Environ. Sci. Technol.* **2014**, *48*, 10354–10362. [CrossRef] [PubMed]

37. Wang, J.; Yan, Z.; Liu, L.; Chen, Y.; Wang, X. In Situ DRIFTS Investigation on the SCR of NO with NH$_3$ over V$_2$O$_5$ Catalyst Supported by Activated Semi-Coke. *Appl. Surf. Sci.* **2014**, *313*, 660–669. [CrossRef]

38. Niu, C.; Wang, B.; Xing, Y.; Su, W.; He, C.; Xiao, L.; Xu, Y.; Zhao, S.; Cheng, Y.; Shi, J. Thulium modified MnO$_x$/TiO$_2$ catalyst for the low-temperature selective catalytic reduction of NO with ammonia. *J. Clean. Prod.* **2021**, *290*, 125858. [CrossRef]

39. Zhang, Y.; Wu, P.; Li, G.; Zhuang, K.; Shen, K.; Wang, S.; Huang, T. Improved activity of Ho-modified Mn/Ti catalysts for the selective catalytic reduction of NO with NH$_3$. *Environ. Sci. Pollut. Res.* **2020**, *27*, 26954–26964. [CrossRef]